Bulletin of the Seismological Society of America, Vol. 97, No. 4, pp. 1212–1220, August 2007, doi: 10.1785/0120060211

Broadening the Response of Short-Period Sensors: An Application to the Sprengnether S-7000 Seismometer

by Elias Th. Koutsoukos and Nikolaos S. Melis

Abstract In this study the application of active damping on a short-period Sprengnether S-7000 passive sensor is presented. This sensor uses a unique magnetic suspension mechanism that eliminates spring resonance effects and ensures improved thermal behavior. The resilient properties of the magnetic spring are devoid of nonlinearities seen in the metallic springs. Although the magnetic suspension is highly susceptible in external magnetic fields, the magnetic scheme applied on the S-7000 seismometer ensures reliable magnetic shielding and it can be considered as a stable suspension. The multiple frequency-dependent feedback, which is the dominant technique in the design of broadband sensors, modified the original velocity response envelop of the old instrument. The theoretical response obtained from the new transfer function, in accordance with the experimental response obtained from calibration data, characterizes the modified S-7000 seismometer as a flat velocity (0.011 to 20 Hz) sensor with top sensitivity 1046 V/m/sec. Amplitude and spectral analyses of datasets obtained from local ground noise, as well as from local, regional, and teleseismic earthquake activity, have been shown to be comparable with respective recordings of other standard broadband seismometers operated at the Athens (ATH) seismographic station vault.

Introduction

The broadening of frequency response of short-period sensors has been approached with several alternative techniques (passive or active) and a variety of technical approaches. Selective amplification of the lower part of the spectrum or direct feedback on the sensing coil has sufficiently increased the low-frequency response of seismic signals recorded by passive short-period sensors (Daniel, 1979; Willmore, 1979; Roberts, 1989). The use of coupled overdamped pendula techniques by Muramatsu *et al.* (2001) achieved wideband response of strong, motion nonfeedback sensors. More recently, simple techniques employing resistance capacitance networks in the place of the classical damping resistance succeed to extend the response of short-period electromagnetic sensors (Pazos *et al.*, 2005).

The application of frequency-dependent feedback on short-period passive sensors is a technique that potentially alters the short-period behavior of the seismometer by filling the loss of the low-frequency content in their frequency response. Usher *et al.* (1979) successfully converted a Willmore Mk IIIa short-period seismometer to a broadband sensor, with the addition of a capacitance transducer and the associated force feedback electronics. However, the conversion of old design seismic instruments using the preceding techniques is not a prescribed solution that can be applied in every case. Moreover, some issues regarding the existing sensor elements and/or technical approaches, such as the calibration or sensing coil, the size weight of the proof mass, the dumping mechanism, the suspension and the available space, all have to be carefully examined before the intervention.

The Sprengnether S-7000 short-period sensor is a seismometer that has been operated for decades in the National Seismic Network in Greece by the Institute of Geodynamics, National Observatory of Athens (NOA). It was deployed in vertical and horizontal orientation (three instruments per station) and operated mostly at 15-analog three-component seismic stations all over Greece from 1965 until 1995 (see NOA Seismological Bulletins).

In our case it was decided to work with the S-7000 sensor (serial no. 4961) oriented vertically. This sensor uses a unique magnetic suspension mechanism that eliminates spring resonance effects and ensures improved thermal behavior. In the mid-sixties and later on, S-7000 was considered as a suspended coil–fixed magnet detector, with an adjustable period range from 0.5 to 1.5 sec and a mass of 1.13 kg intended for both field and observatory operation. The recording and calibration employed two different coils with 27 V/m/sec, 50 Ohms and 0.52 V/m/sec, 3 Ohms, respectively. The damping used fixed resistances in parallel with the recording coil. All these instrument specifications

were considered according to the manufacturer's manual and the calibration sheet of the specific seismometer (Sprengnether, 1965). The S-7000 uses an interesting concentric counterrotating magnet assembly that has a special alloy shunt to compensate for the temperature effects on the strength of the generated magnetic field. The weak point of such magnetic arrangements is the high susceptibility in external magnetic fields. However, because the poles of the rotor magnet are completely inside the stator (fixed magnet), the coupling is relatively immune to external magnetic fields. An initial development of a relative suspension has been reported by Hautly (1964). He described his development as a rotary magnetic suspension system consisting of a hollow cylindrical stator and a rotor magnet magnetically suspended and rotatable within the stator magnet. Figure 1, which is a copy of his original drawing, shows the relation between the stable (A) and the rotatable (B) parts of the restoring magnetic spring. The pivot mechanism (C) is based on crossed hinges, often called Press–Ewing suspension, made from thin strip springs fastened to the chamfered edges of the trunnions and the trunnion cradles.

The study of this unique magnetic suspension, under the precision of a picometer resolution displacement bridge, could explore the properties of this unique magnetic spring and give the possibility for potential operation of the S-7000 sensors as broadband seismometers.

Description of the Modifications Made to the Sprengnether S-7000

No major modifications are needed in the interior of the seismometer, except the addition of the differential capacitance bridge and the associated circuit boards. These parts are fastened in the free space of the seismometer interior. In general, the applied modification does not alter the short-period operation and the initial performance of the S-7000 sensor, in a manner that respects the original design of the instrument.

Figure 2a shows the internal view of the S-7000 seismometer. The instrument is constructed on a huge aluminum base plate. Figure 2a shows the restoring (A) and pivot mechanism (B) formed on the left side of the sensor, and the magnet-coil assembly is formed inside the mass (C). As it is shown in Figure 2b, the vertical aluminum column (D) is originally used by the sensor as mass stopper and also as holder of the optical device that is used for fast leveling of the mass. In the presented modification, this stable part is used to fasten the two circuit boards bilaterally to the midline (Fig. 2b). On the left side (Fig. 2b), the high-frequency and high-impedance stage board (E) is fastened, hence, in the immediate vicinity of the capacitance plates, and the synchronous demodulator and the gain circuitry board (F) is fastened on the right side. Both boards are separately fixed and aligned on the rear face of the vertical column by using a combination of fine screws and glue paste. At the edge of the mass, the transparent part of the optical leveling device is replaced by the movable plate of the capacitance bridge (G). This plate, together with the supporting member, uses the same fasteners as the removed optical part. Thus, the capacitor is placed on the left face of the vertical column and slides in a distance of 0.5 mm. Note that the feedback circuit board can be fastened on either side of the rear free space in the interior of the instrument. However, during the evaluation

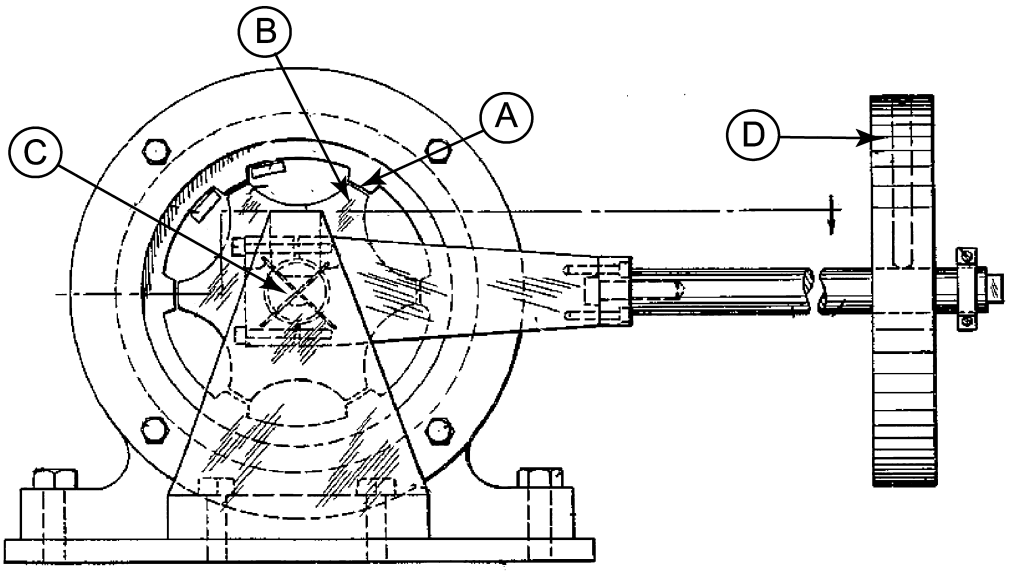

Figure 1. Original drawing of the seismometer invented by R. Hautly appeared in U.S. Patent 3,158,833, dated 24 November 1964. (A) Stator magnet with six radially equally distributed poles. (B) rotor magnet with six radially equally distributed poles in the hollow inner part of the stator magnet. The surfaces of both poles face each other and the formed pole gap is 0.1 mm. (C) Crossed hinges that support the moving part of the pendulum, where the mass (D) is mounted.

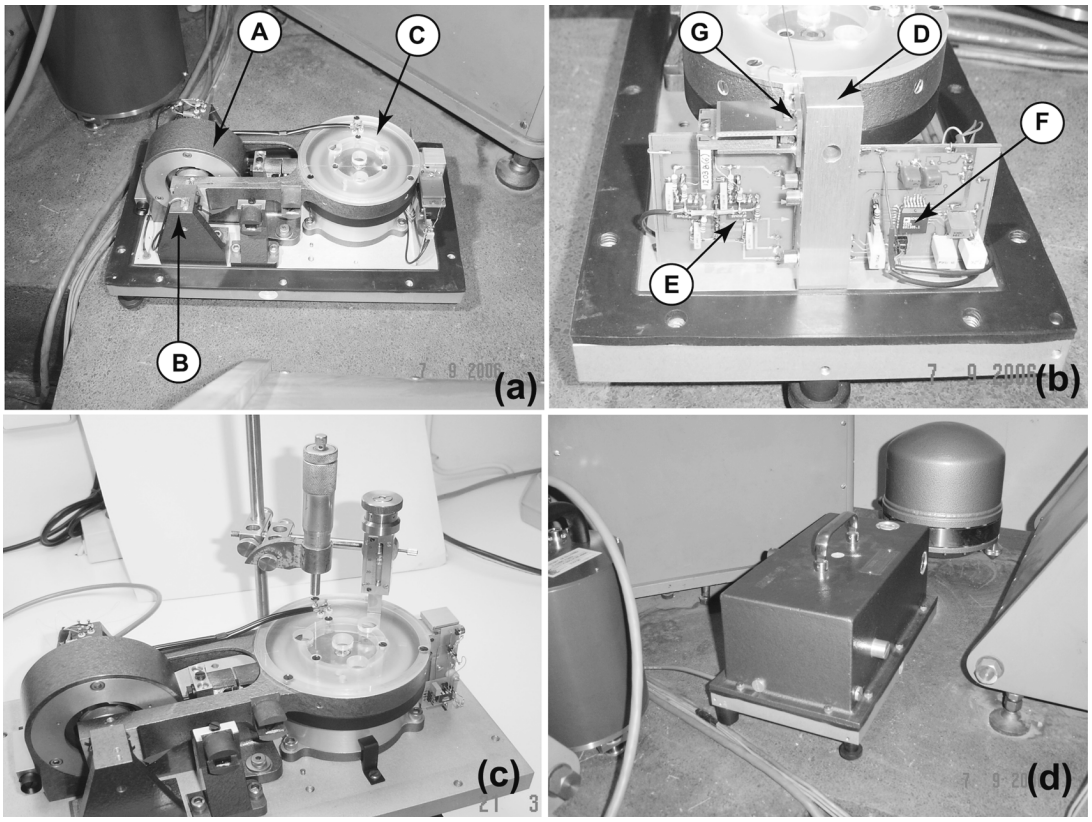

Figure 2. (a) Side-view photograph of the Sprengnether S-7000 seismometer installed in vertical orientation at the ATH seismographic station vault. The magnetic spring (A) is protected against external magnetic influences. The seismic mass (C) is assembled together with the coils of the seismometer and the moving part of the pendulum is pivoted on cradles (B). (b) A close-up view of the electronic module installed on both sides of the stable aluminum column (D). The high-frequency board (E) is fastened to the left of the column, and the synchronous demodulator (F) is fastened to the right. The capacitor is denoted by G, with the moving plates mounted on the mass and in the place where the glass prism was fastened. (c) Photograph that illustrates the seismometer opened during experimentations for the measurement of the critical parameters needed for its transfer function. (d) A wider view of the ATH vault showing the vertical S-7000 (in the center), STS-2 (at the back) and, in part, the short-period WWSSN (to the right) and Guralp 3ESPC (to the left) seismometers.

period, it was decided to keep it outside to freely facilitate the initial adjustments without disturbing the instrument. Figure 2c shows the instrument during testing and measurement of critical parameters related to its transfer function.

For practical reasons, the amplification and synchronous demodulation of the differential capacitance bridge signal employed the AD698AP integrated circuit from Analog Devices. This circuit is a complete monolithic Linear Variable Differential Transformer signal conditioner with reliable characteristics, capable of accommodating the capacitance bridge as input device, following the addition of a differential high-impedance stage to the input. The acquisition and measurement requirements during the development and testing period were supported by a Keithley digitizer and Testpoint (Capital Equipment) software package. The recordings during the evaluation period were made at the Athens (ATH) seismic station (Fig. 2d) of the (HL) Hellenic Broadband Seismic Network, (Melis and Konstantinou, 2006; see also http://bbnet.gein.noa.gr) of the Institute of Geodynamics, National Observatory of Athens. A six-channel DR-24 (Geotech Instruments) 24 bit digitizer was used to acquire the signals of the standard reference instrumentation at the ATH vault (i.e., Streckeisen STS-2, 120 sec, Guralp CMG-40T, 30 sec, and Guralp CMG-3ESP Compact, 60 sec, and modified Sprengnether S-7000 seismometers). MATLAB v6.5 was used as the standard mathematical tool for the study of the sensor dynamics and performance.

Finally, the broadband operation of S-7000 keeps two critical adjustments of the short-period operation: the mass null and the mechanical free-period adjustment. The initial mass position is set through the mechanism that rotates the offset point of the previously mentioned magnet-coupling system. The method although, effective for short-period operation, exhibits some hysteresis caused by the worm–gear system that rotates the stator offset. This point can be conveniently overcome by slow and repetitive adjustments

around the null point. The undamped period is set to 1.7 sec using the existing internal mechanism of the S-7000.

The Suspension of the S-7000 Pendulum

The undamped swinging of the S-7000 pendulum can be characterized by excellent recovery of the null point, after transient or periodic excitation of the boom through the calibration coil. Because its magnetic spring does not suffer from the mechanical nonlinearities and creep phenomena associated with metal springs, as extensively mentioned by Wielandt (2002) and Peters (2006), the long-term stability of the pendulum is defined from the thermal behavior of the magnetic material used for the magnet assembly and the quality of the pivot mechanism.

Even though the specific pendulum design has large mass surfaces exposed in the direction of the relative motion, the corresponding quality factor is close to 8.8, indicating a good suspension. The power spectral density (PSD) of the acceleration caused by the Brownian motion can be derived from the following equation (Aki and Richards, 1980, section 10.3.1):

$$\alpha = \frac{8\pi kT}{MPQ}, \tag{1}$$

where α is the acceleration PSD in $(\mathrm{m/sec^2})^2/\mathrm{Hz}$, $k = 1.38\mathrm{e} - 23$ J/°K is the Boltzmann's constant, T is the absolute temperature in °K, M is the mass in kilograms, P is the resonant period of the pendulum, and Q is the factor characterizing the quality of the suspension. The quality factor describes the energy loss in each cycle of oscillation due to dissipation and characterizes the quality of the suspension and the friction between the moving part of the pendulum and the air.

In the S-7000 the Brownian motion noise was estimated at $1.86\mathrm{e} - 20\ (\mathrm{m/sec^2})^2/\mathrm{Hz}$ expressed in acceleration PSD and has the form of a constant function in the frequency domain. This value is below the new global low-noise model (LNM), in acceleration units, as given by Peterson (1993). Equation (1) simply describes the theoretical thermal noise level of a suspended mass in a standard atmosphere, where the motion is limited by a dissipative damping system. However, the limitations in the detection of the ground motion by the Brownian motion concerns mostly the low-mass designs. In the present study the 1.13-kg mass frames the noise sources in the electronics and the transducer itself. From the preceding analysis, it is derived that the specific pendulum is a quite stable oscillating mechanism. It also exhibits a relatively long natural period, operates with a mass in the range of 1 kg, and the spring used behaves linearly over the extremely limited displacement needed in broadband operation. On the other hand, the relatively long working distance between the point of rotation and the center of the mass offers more linear micro displacement, counteracting the curvilinear motion of the pendulum.

Functional Description

Figure 3 shows a simplified functional diagram of the S-7000 seismometer following the addition of the bridge-detector and feedback electronics. Three different contributions form the current $i(t)$: (1) the proportional current through the resistor R_1, which practically damps the low-frequency oscillation of the system occurring at the lower-frequency corner of the closed loop (at this frequency the differential and integral feedback fail to maintain the equilibrium of the system, because they have opposite phase and cancel each other), (2) the differential current through the capacitor C (the voltage across the capacitor is proportional to ground velocity), and (3) the integral current through the resistor R_2, which is derived from the integration of the output voltage with a time constant τ (this current suppresses the long-period disturbances of the mass). The multiple frequency-dependent feedback is now the dominant technique in the development of high gain and precision broadband sensors and it has been described in detail elsewhere (Usher *et al.*, 1978, 1979; Wielandt and Streckeisen, 1982; Koutsoukos and Melis, 2005).

The transfer function that describes the velocity response of the modified sensor S-7000 is shown by

$$\frac{V(s)}{X_c(s)} = \frac{1}{k_1 C}\left[\frac{s^3 CR_3 + s^2}{s^4\left(\frac{R_3}{k_2 G}\right) + s^3\left(\frac{1}{k_2 GC}\right) + s^2 + s\left(\frac{\omega_0^2}{k_2 GC} + \frac{1}{CR_1}\right) + \frac{1}{CR_2 T_i}}\right] \tag{2}$$

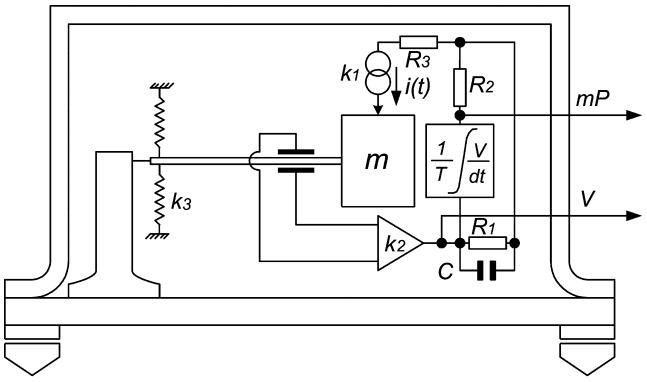

Figure 3. Functional diagram that illustrates the closed-loop control applied on the mass position. An error signal, associated with the position of the inertial mass against the frame of the instrument, is amplified by k_2 and fed to the feedback actuator k_1 through its internal resistance R_3. The total current $i(t)$ is the sum of three different currents passed through R_1, C, and R_2, which is the integrator's output, m is the seismic mass, k_3 represents the stiffness of the magnetic spring, V is the velocity broadband output, and mP is the mass position output signal.

$$h = (2R_1)^{-1} (T_i R_2/C)^{1/2} \quad (3)$$

where k_1 is the displacement constant, 120,000 V/m; k_2 is the feedback motor constant, 27.3 N/A; R_1 is the proportional path resistance, 470,000 Ohm; R_2 is the integrator path series resistance, 305,000 Ohm; R_3 is the feedback coil resistance, 50 Ohm; C is the differential path capacitance, 40×10^{-6} Farad; T_0 is the undamped free period, 1.7 sec; T_i is the integrator time constant, 75 sec; $\omega_0 = 2\pi/T_0$, $G = k_1/M$, and M is the seismometer mass, 1.13 kg. Finally the feedback path closes with the recording coil controlling the mass disturbances.

In Figure 4, the theoretical transfer function based on equation (2), the experimental response curve based on calibration data and the initial velocity response of the seismometer are plotted together. The experimental response curve was calculated after a calibration procedure using the calibration coil of the S-7000 sensor, in combination with a long-period sine wave generator. It was decided to use the velocity as excitation signal of the seismometer by using two different drive methods. In the first method, the coil was driven with constant amplitude signal via a large nonpolar capacitance (array of low-leakage capacitors 100×10^{-6} F total). The calibration current in the second method was corrected by the factor shown in the next equation (4):

$$I_{\text{cal}} = \frac{V_{\text{cal}}}{RT_{\text{cal}}} \quad (4)$$

where I_{cal} is the calibration current, V_{cal} is the amplitude of the calibration signal, R is the series resistance, and T_{cal} is the period of the signal. Both methods led to the same results, ensuring that they can be applied for the investigation of the frequency behavior of the modified S-7000 sensor. As it is shown, the theoretical and the experimental responses are very close, so the theoretical one can be used to characterize the amplitude-versus-frequency response of the sensor. The flat part (0 dB) of the response corresponds to 1046 V/m/sec and the -3 dB amplitudes correspond to 0.011 and 25 Hz, respectively, with damping of 0.709 according to equation (3).

Comparisons of Ground Noise PSD Estimations

Many of noise sources contribute to the formation of the noise envelope recorded at a specific site: (1) the Brownian noise related to the mechanics of the pendulum, (2) the electronic noise as the sum of the whole analog signal conditioning, (3) the environmental noise, and (4) the true ground noise. Even more, the use of integrators for the long-term recovery of the mass position involves additional electronic noise models to those described in detail by Rodgers (1992), regarding velocity feedback seismometers. The first two noise sources are critical in the capability of the sensor to resolve low-amplitude signals, because it is required that the signal resulting from the input exceeds the self-noise of the seismometer, so that the pre-event noise amplitude can be recorded accurately. In the present study, the noise distribution of the modified S-7000 seismometer was estimated by a simple comparison against the noise PSD records obtained from a Streckeisen STS-2 placed on the same pier (in our case, ATH seismic station), which can be considered as a highly sensitive reference instrument. Average noise velocity PSD estimates between 100 and 0.1 sec in period were calculated for the Z components of the Streckeisen STS-2 (120 sec), Guralp CMG-3ESP Compact (60 sec), and the modified S-7000, respectively. The data set selection criteria have been described elsewhere (Wilson *et al.*, 2002; Koutsoukos and Melis, 2005).

Figure 5 shows the noise spectra of STS-2, CMG-3ESP Compact and modified S-7000 seismometers at the ATH vault. Each PSD is the average of five computations obtained

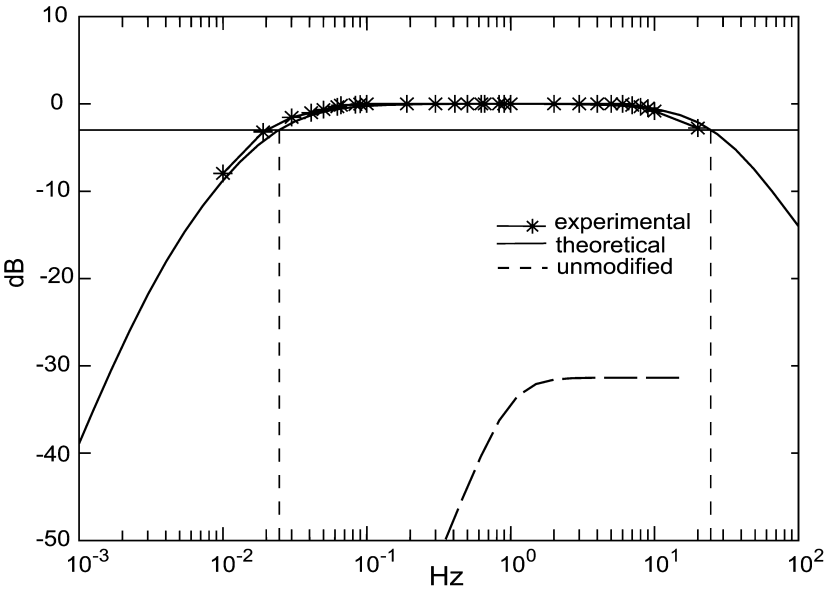

Figure 4. The theoretical response of the modified S-7000 seismometer obtained from the transfer function (solid line), the experimental response curve based on calibration data (asterisks), and the initial velocity response (dashed line).

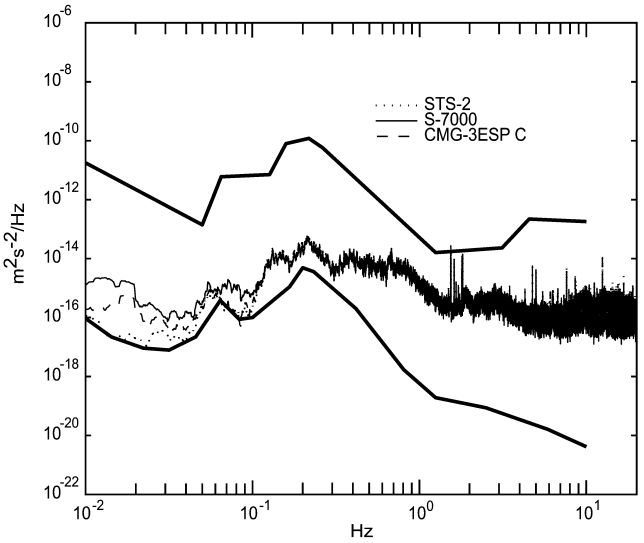

Figure 5. Distribution of the noise power spectral densities at the ATH seismic station. Each PSD is the average of five computations obtained from five, 75% overlapped velocity signal epochs recorded at 50 Hz of 45,000 data points each. Solid, dashed, and dotted lines represent the modified S-7000, CMG-3ESPC, and STS-2 seismometers, respectively.

from five, 75% overlapped, velocity signal epochs, sampled at 50 Hz, with a length of 45,000 data points (900-sec time window). In the same figure are plotted together the new low-noise model (LNM) and the new high-noise model (HNM) curves obtained by Peterson (1993). A peak value in the area of 8.0–9.5 sec indicates the microseismic activity at the ATH station and it has the same pattern for all the sensors compared in the present test. For the period range 10 to 100 sec the STS-2 seems to be quieter than the other two seismometers close together exhibiting morphological similarities in their spectral distributions. A possible interpretation for the differences found in the preceding period range between the two instruments could be the effect of the temperature changes during the recording period, which differently influenced the suspension of the two instruments. For instance, the heavy aluminum base plate of S-7000 could easily produce differential thermal effect with the unshielded cover of the instrument, which, by definition, has different thermal behaviour and should always be thermally isolated. Also, pressure variations can be, and usually are, different in different places on the same pier. In any case, the electronic noise from the integrator could not be excluded in this frequency band.

Comparisons of Teleseismic and Regional Recordings

To evaluate the resolution and the behavior of the modified S-7000 seismometer, several teleseismic and regional events were analyzed during the side-by-side recording period on the ATH vault. Two representative examples were chosen to serve the purpose of the present study, one teleseismic and one regional.

Figure 6 presents velocity records at ATH vault of an earthquake that occurred in Jawa Indonesia (origin time: 17 July 2006, 08:19:28 M_W 7.7, Location: 9.24° S 107.36° E, depth: 10 km), recorded by STS-2 (120 sec), modified S-7000 and Guralp CMG40T (30 sec). The plotted velocity amplitude signals are down-sampled 1-Hz seismograms (Fig. 6a). Two different selected signal windows W1 and W2 show in detail (Fig. 6b, c) two different phases with different frequency content. Amplitude and phase approximately overlay for both sensors with the modified S-7000 to follow the wave configuration pattern of the STS-2 (Fig. 6b, c). The spectral analysis of the selected windows (Fig. 6d, e) indicate similarities in the spectral shape within the range of 0.5 to 0.05 Hz for both instruments, while the differences found in the range of 0.03 to 0.01 Hz could be associated with different low-frequency noise contributions regarding the three instruments.

Figure 7 presents velocity records at ATH vault of a regional earthquake that occurred in Albania (origin time: 8 August 2006 21:20:10, M_W 4.7, Location: 40.17° N 19.78° E, Depth: 10 km), recorded by STS-2, modified S-7000 and Guralp CMG40T (30 sec). In this example, Figure 7a shows the main selected window, and Figure 7b,c shows the zoomed detail window and spectra, respectively. For this regional event, the sampling rate, for both plot and analysis purposes, was 50 Hz. The similarities on the velocity amplitude and the spectral data are the same as with the previous examples shown in Figure 6.

Discussion

Magnetic modules that emulate the behavior of a mechanical spring are capable of being realized under some restrictions. Such developments, when used in sensing devices, are prone to the generation of noise related to the influence of external magnetic fields. However, the closed magnetic scheme in the Sprengnether S-7000 seismometer exhibits reliable magnetic protection of the magnet poles, especially those assembled on the moving part of the pendulum. Following the stator-motor arrangement, applied on the S-7000, the distance between the radially distributed pole-couples is constant, with the rotation of the pendulum changing only the angular position between them. Hence, the exposed pole surfaces of the magnetic assembly always project each other. In general, specialized magnetic shielding of the magnetic spring, using mu-metal or permalloy cover, could significantly eliminate the magnetic susceptibility of the magnetic module in external influences.

The resilient mechanism of the S-7000, although complicated, does not suffer from instabilities that usually concern metallic springs. Sparse inspection of the mass position, bearing in mind that the instrument is installed on a typical WWSSN pier, have shown that the temperature affects the

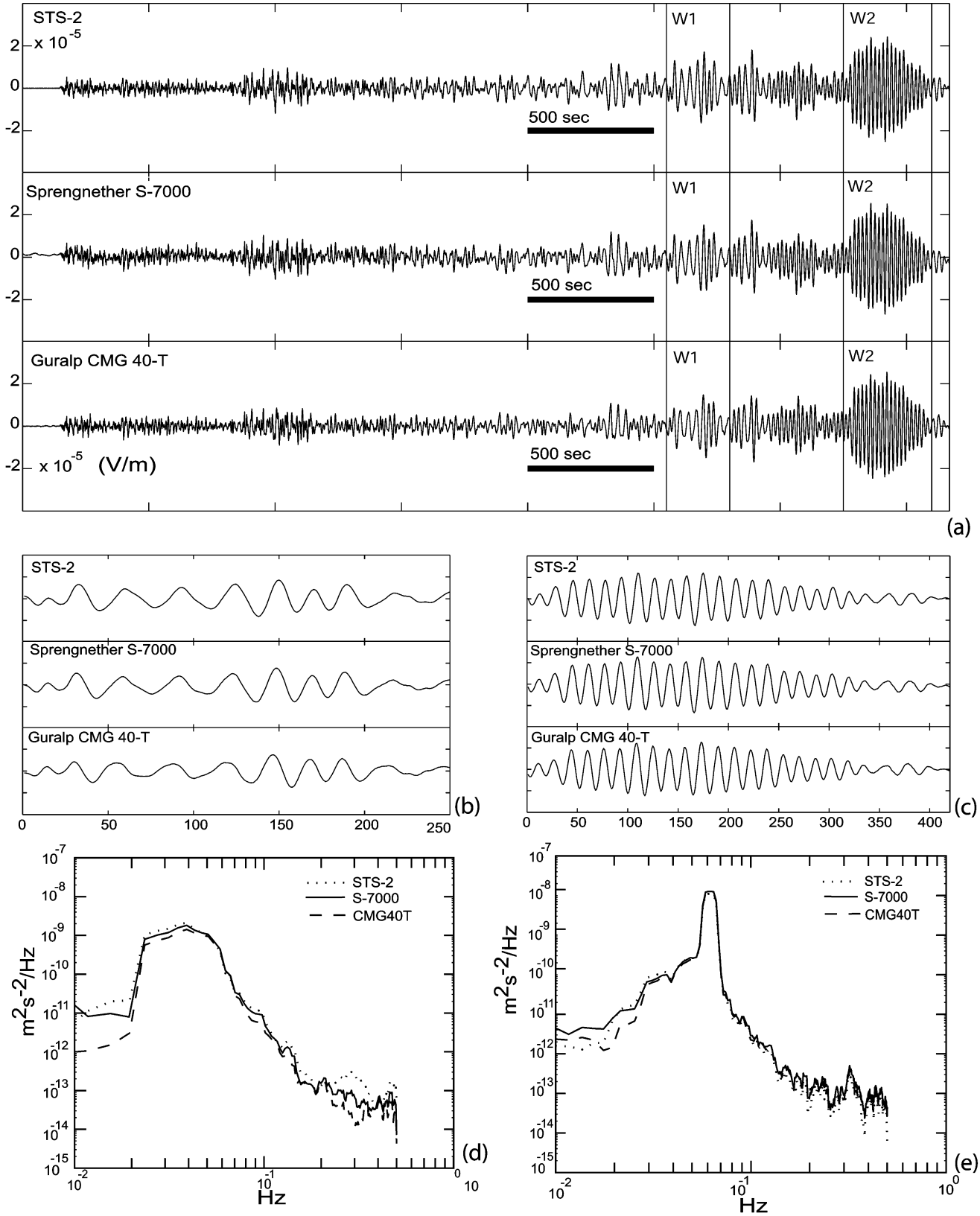

Figure 6. The Jawa, Indonesia, earthquake as recorded at the ATH vault (origin time: 17 July 2006 08:19:28 M_w 7.7, Location: 9.240 S 107.360 E, Depth: 10 km). (a) Velocigrams sampled at 1 Hz; (b, c) the zoomed windows W1 and W2, respectively; (d, e) the corresponding velocity power spectral densities of the zoomed windows. Solid, dashed, and dotted lines indicate the modified S-7000, CMG-40T, and STS-2 window densities, respectively.

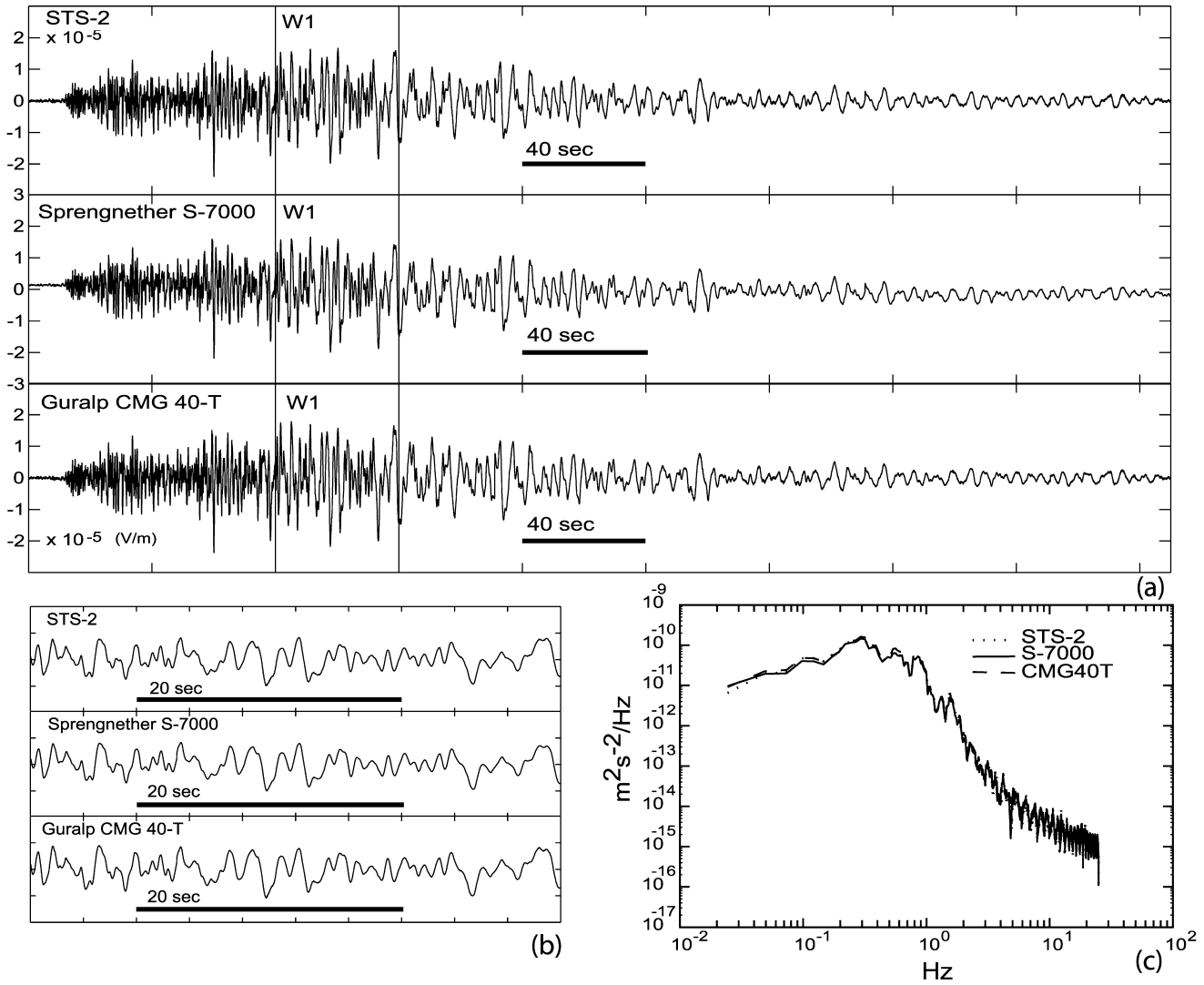

Figure 7. A regional earthquake that occurred in Albania as recorded at the ATH vault (origin time: 8 August 2006 21:20:07, M_w 4.7, Location: 40.170 N 19.780 E, Depth: 10 km). (a) Velocigrams sampled at 50 Hz. The two vertical lines indicate the zoomed window shown in (b). (c) Corresponding velocity power spectral densities of the zoomed window. Solid, dashed, and dotted lines indicate the modified S-7000, CMG-40T, and STS-2 window densities, respectively.

mass position with a seasonal drift of 50 μm per 10°C. The fluctuations of the barometric buoyancy could not be omitted in the lower part of the noise spectrum, where the air tightness of the instrument is not efficient. In this case, the old rubber gasket of the cover should be carefully examined or (better) replaced. On the other hand, some creep observed a few hours after the initial installation of the instrument was attributed to the inaccurate mechanism for the mass positioning used by the instrument. This disturbance can be considered as systematic, because it has appeared each time following the manipulation of the mass position.

The aim of this study was the investigation of the magnetic suspension of the S-7000 under the scheme of a servo system or, in other words, by applying active damping on the pendulum. By maneuvering the parameters of the transfer function that define the response of the closed system, it was possible to operate the old seismometer as a broadband instrument. The response of the modified sensor could be considered as broadband (0.011–25 Hz, 1046 V/m/sec) which is in accordance with the heavy mass, the motor constant of the feedback coil, and the suspension itself. In the present development, characteristics of the seismometer together with the features of the force balance technique were merged following the criticism that has been noted in the literature (Teupser and Plesinger, 1979; Wielandt, 2004). The intervention reached approximately the cost of 600 USD in parts, while a period of two months was consumed for the prototyping and initial bench testing.

Finally, the amplitude and spectral analyses of the local site noise and the regional and the teleseismic activity support that the modified Sprengnether S-7000 seismometer is capable of resolving low-frequency and low-amplitude seismic signals at a permanent observatory deployment.

Acknowledgments

We thank C. Stefanis, President of the Academy of Athens and Director of the Athens University Mental Health Research Institute, for his support and encouragement toward a well-established Laboratory for the Processing of Electrophysiological Signals that made possible the present application. Thanks to G. Stavrakakis, Director of the Institute of Geodynamics, National Observatory of Athens, for his continuous support. We thank Cezar Trifu, Bob Hutt, and Thorne Lay for their fruitful criticism in improving the manuscript.

References

Aki, K., and P. G. Richards (1980). *Quantitative Seismology: Theory and Methods*, Vol. 1, W. H. Freeman and Company, San Francisco, 572 pp.

Daniel, R. G. (1979). An intermediate-period field system using a short-period seismometer, *Bull. Seism. Soc. Am.* **69,** 1623–1626.

Hautly, R. F. (1964). Seismometer, U.S. Patent No. 3,158,833, filed 5 July 1960.

Koutsoukos, E., and N. S. Melis (2005). A horizontal component broadband seismic sensor based on an inverted pendulum, *Bull. Seism. Soc. Am.* **95,** 2462–2471, doi 10.1785/0120050040.

Melis, N. S., and K. I. Konstantinou (2006). Real-time seismic monitoring in the Greek region: an example from the October 17, 2005 East Aegean Sea earthquake sequence, *Seism. Res. Lett.* **77,** 364–370.

Muramatsu, I., T. Sasatani, and I. Yokoi (2001). Velocity-type strong motion seismometer using a coupled pendulum: Design and performance, *Bull. Seism. Soc. Am.* **91,** 604–616.

NOA Seismological Bulletins (1965–1995). Monthly Seismological Bulletins of the Institute of Geodynamics of the National Observatory of Athens, Athens, Greece.

Pazos, A., G. Alguacil, and J. M. Davila (2005). A simple technique to extend the bandwidth of electromagnetic sensors, *Bull. Seism. Soc. Am.* **95,** 1940–1946.

Peters, R. (2006). Damping part I: background and theory, http://physics.mercer.edu/hpage/damping.htm (last accessed September 2006).

Peterson, J. (1993). Observations and modeling of seismic background noise, *U.S. Geol. Surv. Open-File Rept. 93-322*.

Roberts, P. M. (1989). A versatile equalization circuit for increasing seismometer velocity response below the natural frequency, *Bull. Seism. Soc. Am.* **79,** 1607–1617.

Rogers, P. (1992). Frequency limits for seismometers as determined from signal-to-noise ratios, part II: The feedback seismometer, *Bull. Seism. Soc. Am.* **82,** 1099–1123.

Sprengnether, W. F. Instrument Corporation (1965). *Instruction and Maintenance Manual, Variable Period Seismometer, Model S-7000*, Sprengnether Instrument Corporation, Saint Louis, Missouri.

Teupser, C., and A. Plesinger (1979). Design of feedback-controlled wide-band seismographs with respect to undesired side-effects, *Phys. Earth Planet. Interiors* **18,** 58–63.

Usher, M. J., R. F. Burch, and C. Guralp (1979). Wide-band feedback seismometers, *Phys. Earth Planet. Interiors* **18,** 38–50.

Usher, M. J., C. Guralp, and R. F. Burch (1978). The design of miniature wideband seismometers, *Geophys. J. R. Astr. Soc.* **55,** 605–613.

Wielandt, E. (2002). Seismic sensors and their calibration, in *IASPEI New Manual of Seismological Observatory Practice (NMSOP)*, P. Bormann (Editor), Vol. 1, GeoForschungsZentrum Potsdam, 5.6.3.

Wielandt, E. (2004). Design considerations of broadband seismometers, Presentation at IRIS Advanced Broadband Seismometer Workshop, 24–26 March 2004, Lake Tahoe, California.

Wielandt, E., and G. Streckeisen (1982). The leaf-spring spring seismometer: design and performance, *Bull. Seism. Soc. Am.* **72,** 2349–2367.

Willmore, P. L. (1979). Developments in electromagnetic and hybrid seismometers. *Phys. Earth Planet. Interiors* **18,** 35–37.

Wilson, D., J. Leon, R. Aster, J. Ni, J. Schue, S. Grand, S. Semken, S. Baldridge, and W. Gao (2002). Broadband seismic background noise at temporary seismic stations observed on a regional scale in the Southwestern United States, *Bull. Seism. Soc. Am.* **92,** 3335–3341.

Signal Processing Laboratory
University Mental Health Research Institute
P.O. Box 66517
GR-156 01 Papagou, Athens, Greece
E-mail: elkouts1@otenet.gr
(E.K.)

Institute of Geodynamics
National Observatory of Athens
Lofos Nimfon, Thisio, GR-118 10 Athens, Greece
E-mail: nmelis@gein.noa.gr
(N.S.M.)

Manuscript received 9 October 2006.